Available online at www.sciencedirect.com
SCIENCE DIRECT®
Icarus 165 (2003) 223–241
ICARUS
www.elsevier.com/locate/icarus

Tharsis Tholus: an unusual martian volcano

J.B. Plescia

Astrogeology US Geological Survey, 2255 N. Gemini Drive, Flagstaff, AZ 86001, USA

Received 4 April 2001; revised 11 June 2003

Abstract

Tharsis Tholus is unusual martian shield volcano in that the edifice is cut by a series of large normal faults that appear to penetrate the entire volcano. Northeast-trending narrow graben also cut the flank. The large normal faults may be caused by loading of a ductile subsurface layer allowing failure of the edifice; the narrow graben are typical tensional faults. The flank is heavily mantled by aeolian material. Despite the bulbous appearance, the overall morphology of Tharsis Tholus suggests it is a basaltic shield. Crater counts indicate an age of early Hesperian placing Tharsis Tholus in the middle of the period of activity that built the other small Tharsis volcanoes.
Published by Elsevier Inc.

Keywords: Mars; Volcanism; Geologic processes; Surfaces, planets

1. Introduction

Volcanism is the primary geologic process of the Tharsis region of Mars (Carr, 1973, 1974); the area has numerous large central-vent volcanoes with a variety of morphologies that range in size (e.g., Plescia, 2003) from Jovis Tholus (50 × 60 km across) to Olympus Mons (800 km across). In addition to the large structures, there are countless low shields hundreds of meters high and several to tens of kilometers wide (e.g., Sakimoto et al., 2003; Hiesinger and Head, 2002). Aspects of Tharsis volcanism have been studied by many investigators and most of the constructs have been the subject of specific investigations (e.g., Crumpler and Aubele, 1978; Greeley and Spudis, 1981; Cattermole, 1990; Hodges and Moore, 1994; Morris and Tanaka, 1994; Plescia, 1994, 2000; Scott and Zimbelman, 1995; Scott et al., 1998).

The purpose of this paper is to describe the geology and geologic history of Tharsis Tholus, a bulbous-appearing volcano lying on the gentle regional slope in eastern Tharsis. The volcano is ∼ 158 km × 131 km across with a summit caldera complex 48 × 47 km; the long axis of both features is oriented northwest. Tharsis Tholus exhibits the unique attribute of large normal faults having hundreds of meters of offset that cut across the entire flank and presumably through the entire edifice. No other martian volcano exhibits such faulting. Tharsis Tholus, like other smaller Tharsis volcanoes, is surrounded and partly buried by younger lavas and has a caldera that is relatively large compared with terrestrial volcanoes.

2. Previous work

Previous mention of Tharsis Tholus (Fig. 1) has typically been in the context of broader studies. Carr (1975) mapped it as cratered shield material, a unit to which he assigned all of the small volcanoes within the Tharsis 1:5,000,000 quadrangle. Scott et al. (1981) assigned Tharsis Tholus to Amazonian–Hesperian undivided volcanic material. Scott and Tanaka (1986), in their 1:15,000,000 map of the western hemisphere, simply mapped it as an undifferentiated volcano. Greeley and Spudis (1981) suggested Tharsis Tholus is a dome based on the assumption that it has steep flank slopes and a convex profile. Robinson (1993) reviewed its geology and concluded, based on its morphology, that it was probably built dominantly by explosive volcanism. Hodges and Moore (1994) suggested that the volcano is a basaltic shield. In their study of the various types of volcanic calderas on Mars, Crumpler et al. (1996) cited Tharsis Tholus as the best example of a volcano with sector structure having large-scale faulting and slumping.

E-mail address: jplescia@usgs.gov.

0019-1035/$ – see front matter Published by Elsevier Inc.
doi:10.1016/S0019-1035(03)00199-4

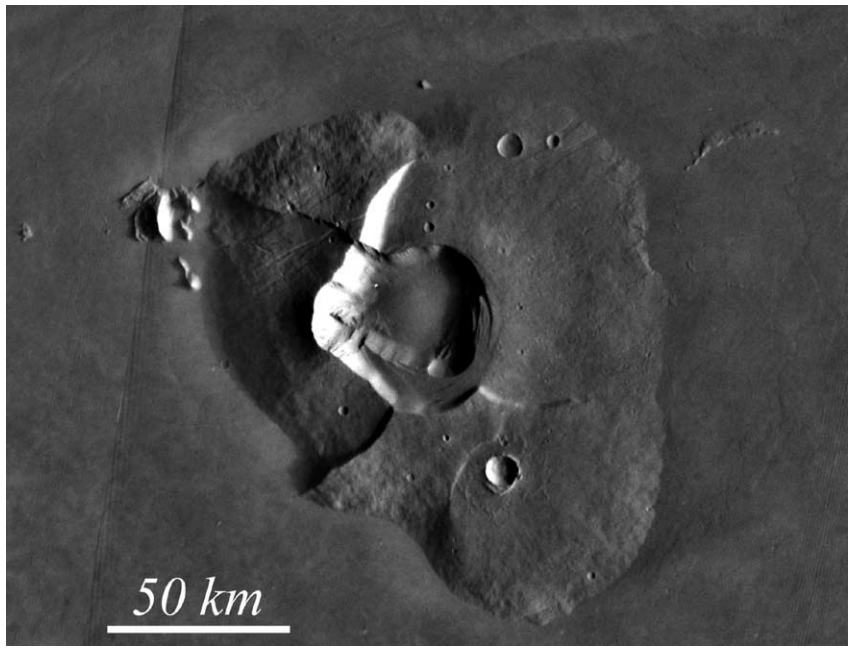

Fig. 1. Large normal faults cut the flanks to the north-northeast, east, southwest and northwest of the caldera and a fault cuts up across the southern flank. Note blocks at the base of the northwest flank, knobs of basement with circular outline protruding through lavas east of the volcano, and the dark wind streak extending to the northeast of the volcano. Viking images 858A21, 23, 186 m/pixel; north is at the top.

3. Morphometry

MOLA data (Zuber et al., 1992; Smith et al., 2001), MOC images (Malin et al., 1992; Malin and Edgett, 2001), and THEMIS data (Christensen et al., 1999) allow a more complete understanding of the geology of Tharsis Tholus to be developed than was possible with Viking images and Viking-era topography (e.g., US Geol. Survey, 1989, 1991). Numerous studies have already taken advantage of the MOLA data to assist in the interpretation of the geologic and structural history of martian volcanoes (e.g., Head et al., 1998a, 1998b; McGovern et al., 2001; Mouginis-Mark and Kallianpur, 2002; Plescia, 2003).

The basic MOLA data set of individual orbits was used to compile a digital elevation model of Tharsis Tholus (Fig. 2). Data covering the region were extracted and then gridded. Bad and overlapping tracks were removed from the data base to eliminate noise and spurious spikes caused by the gridding. A 500 m grid spacing was used for the DEM.

The volcano exhibits considerable relief across its surface. Maximum elevation is just over 9 km on the flank immediately to the west of the caldera rim. Plains to the west have an elevation of 2.2 km, whereas those to the east have an elevation of about 1.1 km, thus the volcano stands 7–8 km above the surrounding region. Tharsis Tholus has clearly acted as an obstruction to lava flows extending down slope to the northeast from the interior of the Tharsis region. There is almost a 1 km elevation difference between plains on the northeast and southwest margins of the volcano and lava flows are observed to flow around the structure and to be ponded on the southwest side. The northeast regional slope is $< 0.2°$ that would suggest plains elevation differences of only a few hundred meters across the edifice. Thus, the larger elevation difference reflects the thickness of the lavas ponded against the southwest side of the volcano.

Along the western caldera rim elevations increase from 7.5 to 9 km and then down to 6.6 km; along the eastern edge of the caldera the elevations are more constant at about 4.8 to 5.3 km. Maximum elevation on the north flank is 8.3 km and about 7 km on the south flank. The elevation of the caldera rim on the east side is lower, at about 5 km. Most of the caldera floor lies at an elevation of about 2.2 km. The western part of the floor rises from 2.2 to 3.2 km toward the western wall. This area has been mapped as a landslide (see below). Relief from the caldera rim to the floor varies from almost 7 km on the west wall to about 2.5 km on the east wall. Robinson (1993) suggested the western caldera wall was at least 4.2 km high, the eastern wall at least 2.5 km, and that the caldera floor lay about 1 km below the surrounding plains. The MOLA elevations place the floor just above the level of the exterior plain, rather than 1 km below.

US Geol. Survey (1989, 1991) stereogrammetry-based topography of the volcano indicated flank slopes of $\sim 6°$, although locally they could have been as large as 12°. Robinson (1993) suggested that slopes might approach 16° on the northwest side based on shadow measurements. MOLA data indicate that slopes are variable around the flanks and with elevation (Table 1). Figure 3 shows the topography and slopes along northeast-southwest and northwest-southeast profiles across the volcano. A convex shape is clearly shown by the profiles. Slopes are greatest at the base of the flank and decrease toward the summit (Fig. 4). Mean slopes (cal-

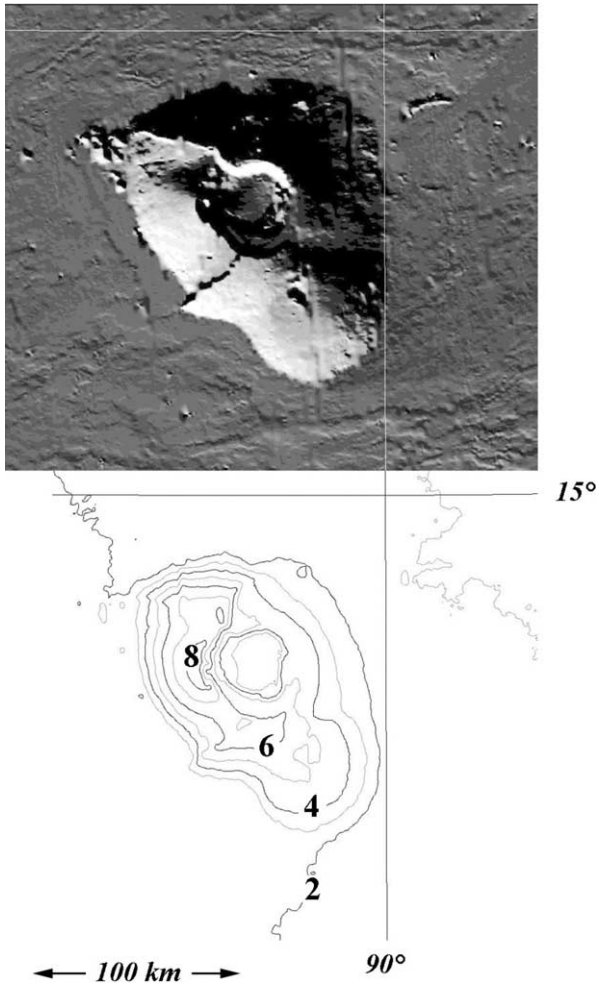

Fig. 2. MOLA based shaded relief and topography. Upper panel shows shaded relief with illumination from the south. Lower panel shows contour map with 1 km contour interval, every other contour is highlighted. North is at the top.

Table 1
Mean slope, RMS height and RMS slope for Tharsis Tholus flanks

Flank	Mean slope°	RMS height	RMS slope°
East	6.13	3361	6.13
North	13.94	1465	14.15
Northeast	6.62	1622	6.97
Northwest	12.88	3061	13.86
Southeast lower	7.85	541	8.71
Southeast upper	3.34	1545	3.48
Southwest	15.03	1410	15.44
West	12.71	1701	17.54

Mean slope was calculated using data from profiles extending through the DEM over distances of 1 km. RMS height and slope were calculated using the equations presented in Shepard et al. (2001) and the DEM profiles.

culated over a few MOLA shot points) are highest on the north and west flanks reaching 12°–15° similar to Robinson's data. Steeper slopes at the base and gentler slopes near the summit (about 3°) are well illustrated in Figs. 2 and 3.

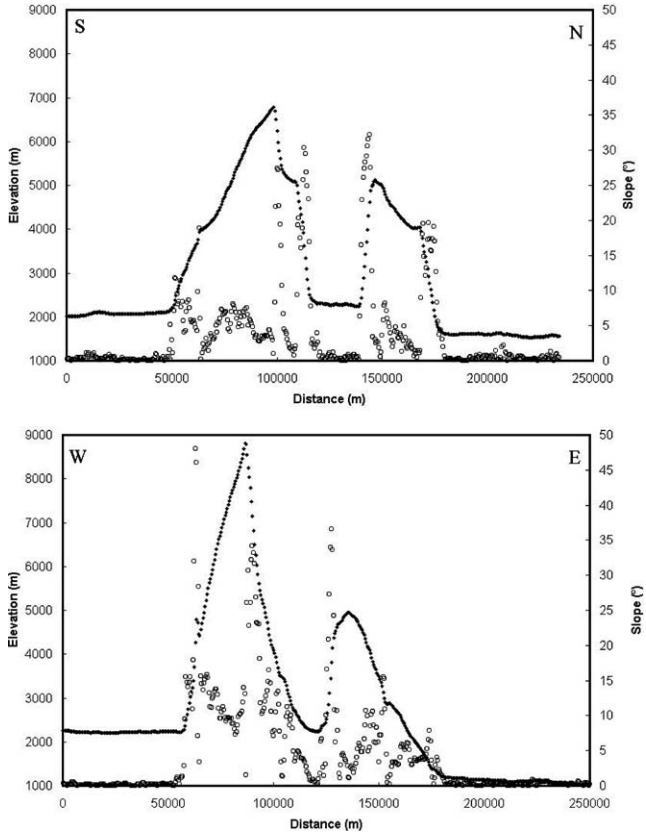

Fig. 3. Northeast–southwest profile showing topography and slope (upper). Southeast–northwest profile showing topography and slope (lower). Small + symbols denote the elevation, open circles o denote the slope. Vertical exaggeration is about 21X.

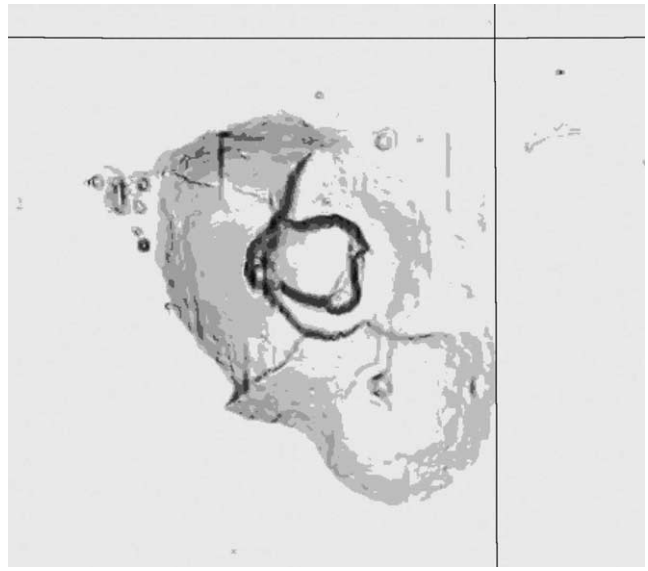

Fig. 4. DEM derived slopes; bright shades indicate low slopes; darker shades indicate steeper slopes. Note flat plains and steep slopes on the faults and on the interior of the caldera walls.

4. Geology

This interpretation of the geology of Tharsis Tholus (Fig. 5) is based on an analysis of Viking, MOC and THEMIS images. Appendix A lists the images used in the study and their associated data. Most of the volcano is mapped as a single unit termed "flank material" because the thick mantle obscures the details of the underlying surface and prevents discrimination of additional units. Tharsis Tholus is surrounded by volcanic plains that are mapped as part of Member 5 of the Tharsis Montes Formation (Scott and Tanaka, 1986). The caldera complex includes caldera wall material (cw), two caldera floor surfaces (cf_1, cf_2), and landslide material (ls). A small patch of plains (p) is mapped surrounding the blocks at the base of the northwest flank. To the east and north of the volcano, exposures of basement (b) protrude through the lavas. Those to the east have a circular pattern that is interpreted to be a buried impact crater. Figure 6 illustrates the location of the MOC and Viking images referenced below.

4.1. Flank

The flanks of Tharsis Tholus (Fig. 6) exhibit a hummocky texture, a few troughs, narrow graben, and the large normal faults that divide the volcano into five major blocks (Figs. 1, 5). Robinson (1993) also noted that the flanks were smooth to hummocky and lacked recognizable lava flows; he also reported that it lacked valleys (as occur on Ceraunius Tholus) although several are reported here.

The lack of morphologic detail observable in Viking images suggested the surface was heavily mantled. That impression is clearly borne out in the MOC images which show extensive mantling of the surface (Figs. 7 and 8). The mantling of the volcano is in sharp contrast to the relatively pristine nature of the surrounding plains. MOC images showing the volcano-plains contact (e.g., M03-05935, M03-00801) and those of the nearby plains show the plains are considerably less mantled such that their volcanic morphology and small-crater populations can be clearly observed.

As suggested by Crumpler et al. (1996) the degree of mantling is variable. They suggested the eastern flank was smoother than other sectors and that the north and south flanks were rougher. For example (Fig. 7), on some parts of the flank (e.g., northeast and western margins) narrow graben are quite distinct; elsewhere their appearance is subdued (e.g., southern flank). Craters are filled to different degree and small-crater ejecta blankets are rarely observed. Pieces of the underlying volcanic surface are either exposed or only thinly mantled in scattered locations. Variability is also expressed in the frequency of relatively fresh small-diameter craters (< 50 m) which vary across the surface. Mantling material is also drifted against the large normal faults scarps and along the contact of the flank with the plains.

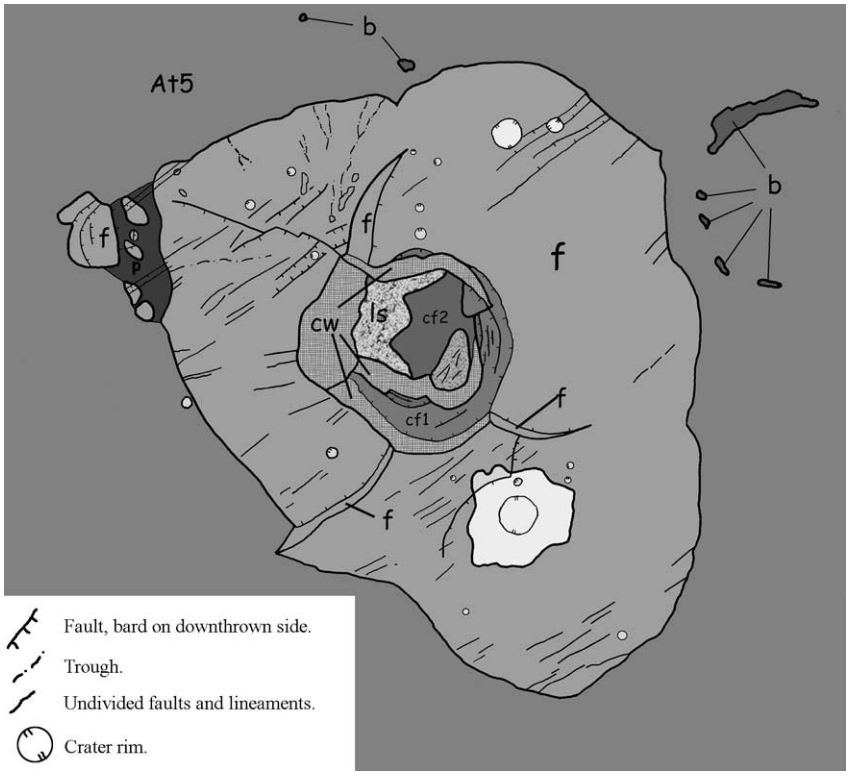

Fig. 5. Geologic sketch map of Tharsis Tholus. Units include: f: flank material; At5: Member 5 of the Tharsis Montes Formation; cw: caldera wall material; cf_1: caldera floor material 1; cf_2: caldera floor material 2; ls: landslide; b: exposures of pre-plains bedrock; p: plains units; light areas denote crater interiors and crater ejecta.

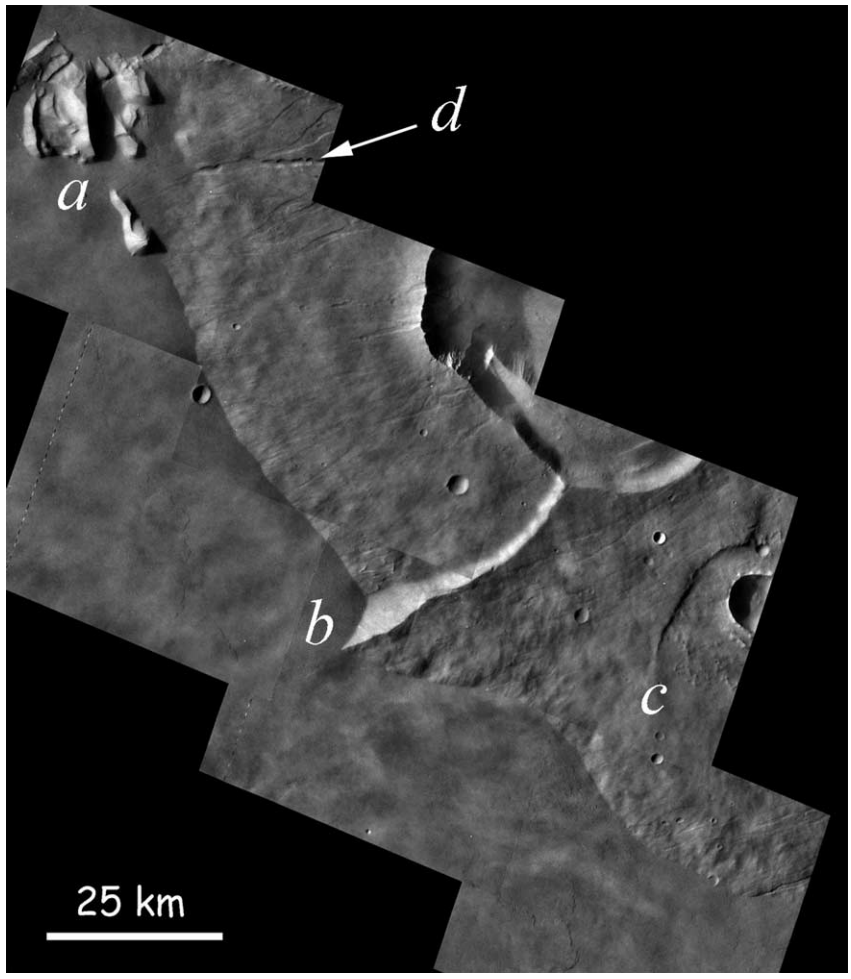

Fig. 6. Western flank of Tharsis Tholus (mosaic of Viking images 699A11-16; 36 m/pixel). Narrow, northeast-trending graben cut much of the flank. Faulted blocks at base of northwest flank (a), southwest normal fault (b), normal fault cutting south flank (c), and trough with curvilinear margins (d).

Mantling material has several morphologies (Fig. 8); it can appear smooth, granular, or have a linear to rectangular appearance. The linear and rectangular appearance is interpreted as a surface covered with dunes. In other locations, a patchy surface texture suggests material is being striped away rather than transported across the surface as dunes. The variability morphology and the range of preservation states of small-diameter craters suggest the surface is in some form of equilibrium between small-diameter cratering and the deposition and erosion of the mantling material, rather than the mantling being a discrete event.

The absence of widespread bedrock exposures is also indicated by night-time THEMIS imaging. Figure 9 shows three night time (12.57 micron) strips across the volcano. Most of the surface has a relatively dark tone indicating a cool, low thermal inertia surface (e.g., mantling material). Only along portions of the rough western caldera wall, along the top of northern edge caldera wall and the rim of the large (8.8 km) impact crater on the south flank and some of the smaller impact craters are warm surfaces (high thermal inertia), suggesting the presence of exposed bedrock, observed. The large fault scarps that cut the flank are slightly warmer than the surrounding areas but not as warm as the locations noted above, possibly indicating the presence of pieces of bedrock exposed within the debris along the scarp rather than in place bedrock exposed along the fault scarps. However, some of graben along the southern flank are warm (Fig. 10c) suggesting the presence of exposed rock along those scarps.

Despite the clearly volcanic morphology of the surrounding plains and the large-scale volcanic character of Tharsis Tholus, lavas flows are not clearly observed on the flanks in either Viking or MOC images. The morphology observed in the high-illumination angle MOC images is dominated by the mantle. However, two THEMIS images, one of the southern flank and the other of the summit region (Fig. 10) show linear topographic highs extending down slope. Similar linear features are observed in the Viking images of the western flank (Fig. 6). The topography and morphology of these features suggest they are heavily mantled lava flows.

Troughs are observed in several locations on the western and northern flanks and are either hidden or absent elsewhere. They are several hundred meters to just over a kilometer wide. Figure 7a shows one on the northern flank

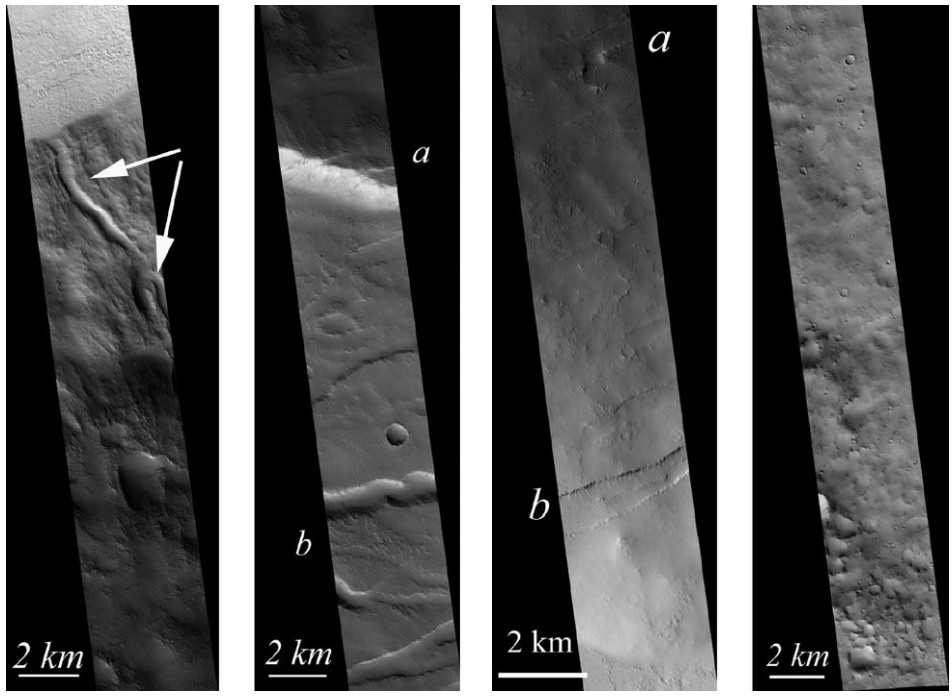

Fig. 7. Flank morphology. (a) Base of northwest flank showing branching trough (500 m across; 8.5 km long) and mantled surface (MOC E09-01814, resolution 6.21 m/pixel). (b) Upper northwest flank crossing the northwest normal fault showing mantling, infilling of craters and graben and drifting against the scarp and a meandering trough about 990 m wide (MOC E09-01814, resolution 6.21 m/pixel). (c) Upper southern flank showing heavily mantled (a) and less mantled (b) northeast-trending graben (MOC M03-05935, resolution 5.86 m/pixel). (d) Southeast flank margin (MOC E12-01907, resolution 6.2 m/pixel) showing mantled surface at the top of the strip and less mantled (more cratered) surface at the bottom. North is at the top is all images.

above the contact with the surrounding plains. The trough is about 900 m wide; two troughs extend down the flank and merge into a single trough that extends to the contact with the plains. It has levees on both side of the channel. Figures 6 and 11 show other troughs on the western and northern flanks, respectively. The western flank has a trough that extends more than 20 km down the flank. It is 700–1300 m wide and has a curvilinear margin. Troughs observed extending down the north flank (Fig. 12) are about 500 m wide and begin at irregular shaped depressions high on the flank.

The morphologic attributes of the trough, such as a single channel of uniform width, levees, lack of tributaries, and restricted occurrence, are more suggestive of a volcanic than a fluvial origin. However, many of the channels on Ceraunius Tholus (Plescia, 2000) have morphologies similar to those on Tharsis Tholus, and the Ceraunius troughs have been interpreted as fluvial in origin (Gulick, 2001).

Immediately adjacent to the northwest flank is a group of north- to northeast-trending blocks (Figs. 1, 13). These are almost certainly related to Tharsis Tholus rather than being pieces of unrelated older pre-volcanic bedrock protruding through the plains. The group extends over an area of 30×25 km with individual blocks being up to 15 km long and 12 km wide and 300–1100 m high. Some scarps show layering. Block geometries suggest that they have been broken up by faults of variable strike. The blocks are embayed by a plains unit that is younger than the volcano but older than the regional volcanic plains. This plains unit is cut by the northeast-trending graben.

Crumpler et al. (1996) suggest the blocks might represent slide material derived from the volcano flank. The blocks do resemble, at least superficially, landslides shed from the Hawaiian islands, particularly those north of Oahu—e.g., the Nuuanu landslide (Moore et al., 1989, 1995; Naka et al., 2000). However, there is no obvious source on the flank. It is possible that the source area for the landslide now lies buried beneath younger flows. Alternatively, the blocks could represent a portion of the flank that was disrupted in a more random manner during the formation of the adjacent northwest-trending normal fault. An another possible explanation is that the blocks were formed by a thrust fault ramping up from beneath the edifice (see below), but the variable strike of the faults that break the blocks might argue against such a model. Finally, they could represent the surface manifestations of a shallow intrusion such as a laccolith. There is, unfortunately, insufficient data to discriminate among the models.

Rimless pits are observed in a few locations on the flank. Several large pits occur on the northwest flank, there, a large pit (3.4×1.6 km) is centered over a northeast-trending graben (Fig. 12). Two additional pits (~ 1–1.2 km $\times 0.7$ km) occur in a graben on the southwest flank. The association of pits with the graben suggest they are collapse features related to the extension expressed by the graben. Graben and

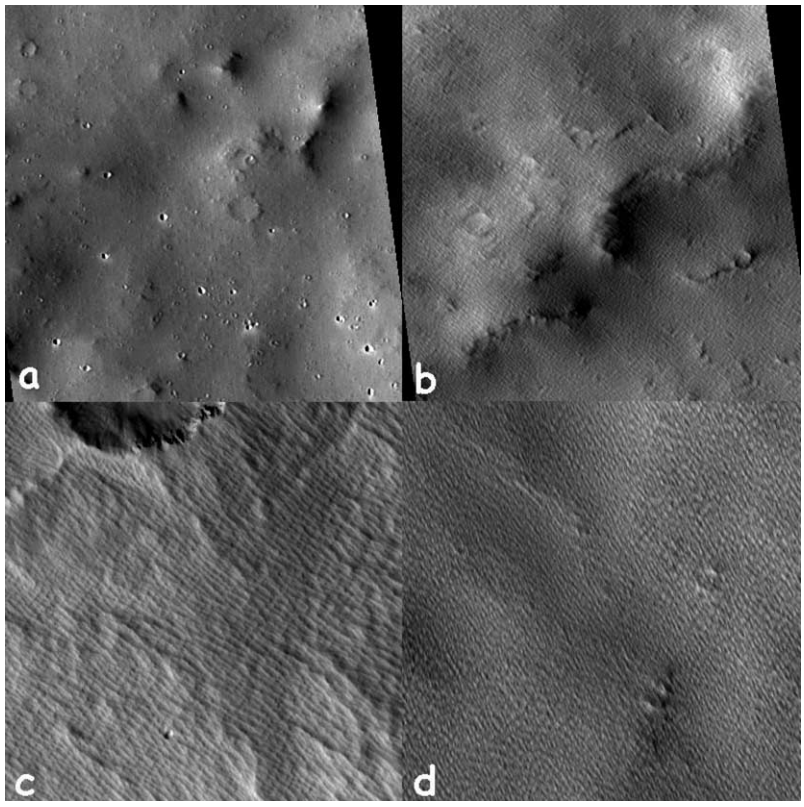

Fig. 8. Flank mantle morphology. Note the variation in frequency of small impact craters and the degree to which larger craters are in filled. (a) Smoothly mantled surface. Small areas of the underlying flank material are either thinly or unmantled (MOC M03-00801). (b) Mantled surface with low relief rectilinear pattern. Small areas the underlying flank material are either thinly or unmantled (MOC M03-00801). (c) Distinct northwest and northeast trending sculpting of mantled surface (MOC M03-04592). (d) Mantle with granular texture (MOC M03-05935). This texture may represent a very subdued example of the rectilinear texture in (c). MOC image M03-00801 has a resolution of 7.36 m/pixel and M03-05935 has a resolution of 2.94 m/pixel. North is at the top.

pits are often found together in Tharsis such as in Tractus and Acheron Catena near Alba Patera. Presumably these pits are formed due to collapse of surface material into cracks as observed on Kilauea (Okubo and Martel, 1998). A number of small, elongate pits are observed on the eastern flank (Fig. 14), but these appear to be secondary craters.

4.2. Caldera complex

The caldera's outline is relatively circular and it is composed of two overlapping calderas (Figs. 5, 15)—an outer older one and an inner younger one. Map units include wall and floor materials. Wall material (cw) is presumably exposed lava flows and possibly other volcanic material (e.g., pyroclastics or intrusions). The upper caldera walls form cliffs with a spur and groove morphology interpreted to indicate the presence of exposed bedrock (Figs. 15 and 16). Farther down slope the material appears to be talus which in some places feathers onto the caldera floor without an abrupt contact. The talus locally has an interesting morphology composed of linear parallel ridges and troughs tens of meters wide, spaced 100–200 m apart and about 1 km long suggestive of erosion. In other locations the talus surface appears smooth.

The older, outer caldera is $\sim 48 \times 47$ km across and is defined by a piece of the floor (cf_1) preserved along the southern margin of the younger caldera and in a small sliver on the north side. It is bounded along its exterior margin by inward-facing normal faults. On the east side, the floor is broken into blocks down-dropped along parallel faults. Most of this unit is smooth and mantled and lies at an elevation of ~ 5.1–5.2 km.

The younger inner caldera has a diameter of $\sim 41 \times 40$ km. It is fault bounded on all sides except the west. The floor is composed of two units, floor material (cf_2) and landslide material (ls). Unit cf_2 presumably represents the original caldera floor formed during the last episode of caldera volcanism and later modified by mass wasting and aeolian processes. It is a level (~ 2.2 km), mantled surface, locally covered with dunes; there are no obvious volcanic morphologies. A well-defined contact between the caldera floor and walls does not always occur. Although it is mantled, the floor material is either older or more thinly mantled than the flank as a significant numbers of small impact craters are observed. Landslides have affected the south and western margins of the caldera. A large alcove on the south side, within which is a jumbled slide deposit, formed by the failure of the older floor (Fig. 15).

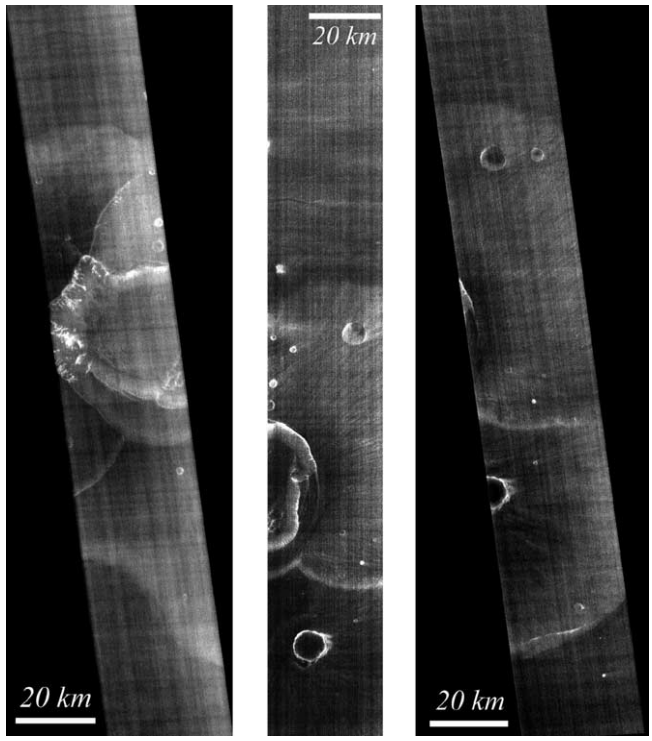

(a) (b) (c)

Fig. 9. THEMIS night-time (12.57 micron) images of Tharsis Tholus. (a) Northern flank, caldera and southern flank (I02319005). (b) Eastern part of the caldera, the northern flank and the upper part of the south flank. This strip is not reprojected due to missing geometry data (I01233003). (c) Eastern flank. The crater on the southern flank is the same one that is observed south of the caldera in B (I00871005).

The western caldera wall has a rough morphology and four large alcove-shaped re-entrants separated by long spurs of bedrock (Figs. 15 and 17). The upper caldera wall is characterized by ridges and spurs ∼ 500 apart; layering is apparent in the walls. THEMIS data (Fig. 9a) suggest the presence of bedrock along the ridge lines. At the base of the wall is a hummocky deposit extending onto the caldera floor that is mapped as landslide material (ls). Elevations rise across the landslide deposit from 2.2 km at its eastern edge to 3.2 km against the western wall, suggesting the apron of material could be a kilometer thick at the base of the wall. The rough morphology of the western wall is consistent with a landslide scar. Presumably the original west caldera margin was formed by a fault that extended in a simple arc around the western side of the caldera merging with the fault traces on the southwest side.

5. Structure

Two types of tectonic features are observed on the flanks of Tharsis Tholus: narrow, northeast-trending graben (Figs. 6, 7, 10, 11, 14) and large normal faults (Fig. 1). Neither fault type cuts the surrounding plains indicating that flank deformation predates the emplacement of those plains.

5.1. Normal faults

There are five major normal faults cutting across the flanks each having large offsets. Four of them extend from the caldera: north–northeast (azimuth 18°), east (110–120°), southwest (225°), and northwest (294°); a fifth cuts across the southern flank from the southeast fault (210°). The length and offset suggest these faults cut the entire edifice. Individual scarps have exposed lengths of 30–60 km and extend from the summit down the flank. The northwest and southwest fault scarps extend from the summit all the way to the base. Those on the east and south sides are not exposed all the way to the contact with the surrounding plains and appear to be buried at their distal ends by younger flank lava flows. The fault on the south flank is also partly buried. MOLA data indicate the scarps are several hundred meters to a kilometer high with the height decreasing down slope.

The distal ends of the faults on the east side are clearly buried by younger flank materials (Fig. 11). Geologic relations are consistent with two possible timings. All of the faults formed at the same time and later volcanism on the eastern flank buried the distal ends of the north–northeast and southeast faults. Or, the faults on the east side formed, widespread volcanism occurred and then the faults on the west side formed.

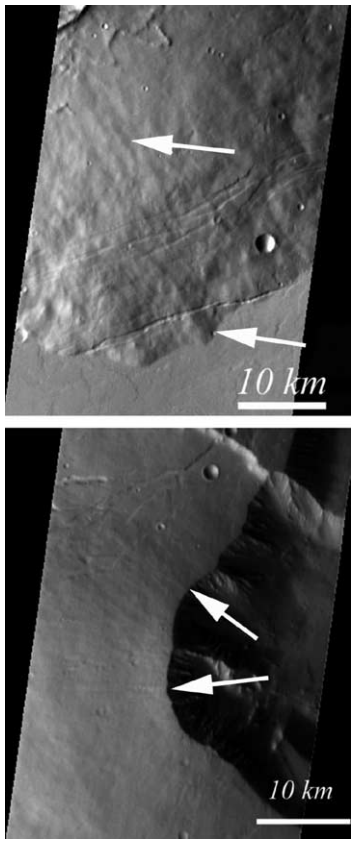

Fig. 10. THEMIS images showing linear topographic highs extending down the flank interpreted to be mantled lava flows. A few locations are highlighted with arrows. Upper panel shows the southern flank with linear features extending southeast down the slope. It also shows northeast-trending graben cutting the flank at the base and about a third of the way up the flank (THEMIS I02200005, resolution 100 m/pixel). Lower panel shows the area to the west of the caldera with a radial pattern of linear highs extending away from the caldera edge. Also shown is a portion of the northwest normal faults and small northeast-trending fractures (THEMIS I01164006, resolution 100 m/pixel).

Fig. 11. THEMIS image (I01863002, resolution 100 m/pixel) showing the northern flank of Tharsis Tholus and the north-northeast trending normal fault. The distal down slope end of the fault is covered by younger lavas from the summit region. Note also the northeast-trending graben and the narrow troughs extending down the flank.

The east and western flanks are down dropped relative to the north and south flanks, a geometry similar to the northeast trending graben. The decrease in scarp height along strike for the normal faults on the east flank suggest that the portions near the volcano margins are buried by younger lavas, that the faults have a scissors-type motion with increasing displacement up-slope toward the caldera, or the there is a lateral component of motions as well such that the east and west blocks moved both down and out relative to the north and south blocks.

5.2. Graben

Narrow graben cutting the volcano are observed on all but the eastern flank, although this may be an observational bias (lack of appropriate imaging) rather than a lack of faulting. The general trend is northeast but the strikes can be variable. Graben on the north flank strike 50° N–65° E, those on the west flank 45° N–70° E, and those on the south flank 35° N–70° E with some having distinctly curvilinear trends. Widths range from a few hundred meters to ~ 3 km; typical widths are 500–600 m. Some graben are quite irregular; for example a graben on the northwest flank varies in width from ~ 1 km to 2.8 km over a distance of 12 km. A number of additional linear features occur on the flank that are interpreted to be unresolved or buried graben. The degree of mantling is sufficient to obscure some of the graben (Fig. 7). These observations are similar to those noted by Robinson (1993).

Most graben are simple, having a single scarp on each side. Some graben on the north flank have multiple bounding faults. Graben on the southern flank are narrower than those on the north flank. The observed widths suggest that the graben-bounding faults intersect at depths of < 1 km (assuming a 60° dip on both faults). Thus, some aspect of the internal layering of the volcano controls the style nature of faulting rather than the entire edifice.

The age relation between the normal faults and the northeast trending graben is complex. In each location where the surface is observed with sufficient resolution, the northeast-

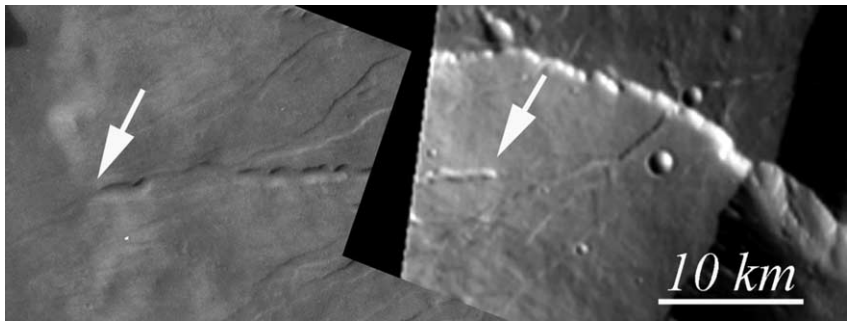

Fig. 12. Trough with curvilinear margins extending down the west flank. Arrows denote proximal and distal ends. Viking image 699A10 and THEMIS image I01164006.

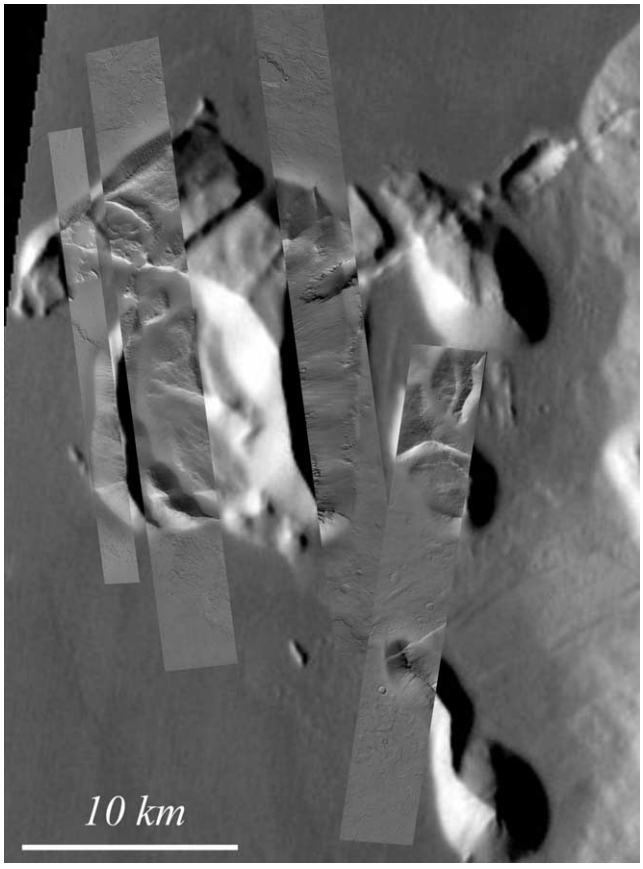

Fig. 13. Blocks at the base of the northwest flank. Blocks are embayed on the west and north by younger regional volcanic plains and on the east by an older faulted plains unit that is younger than the blocks and the construct, but older than the regional plains. Note narrow, northeast-trending graben that cut the blocks and the plains between the blocks and the flank, but not the surrounding plains. THEMIS base image (I01888005, resolution 100 m/pixel) with MOC images M08-04702 (resolution 2.94 m/pixel), E13-00672 (resolution 6.2 m/pixel), E12-00031 (resolution 4.66 m/pixel), SP1-23106 (resolution 3.15 m/pixel) overlain. North is at the top.

trending graben cut the normal faults, indicating the graben are younger. However, the northwest normal fault has a trace which locally has a northeast strike (Fig. 5) indicating that it has been influenced (i.e., is younger) by northeast lines of weakness. This suggests that northeast trending graben formed repeatedly over an extended period.

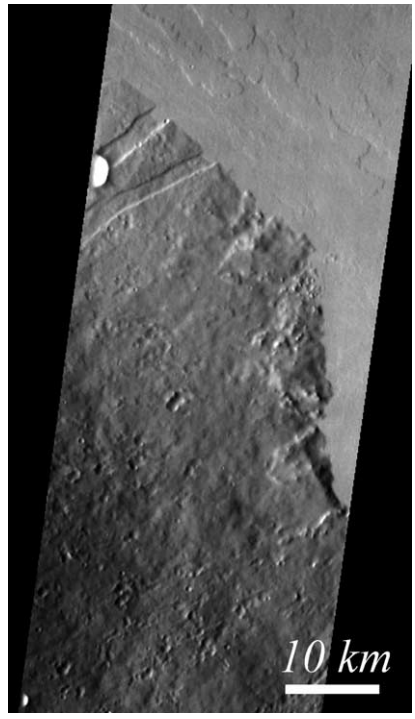

Fig. 14. THEMIS image (I02200005, resolution 100 m/pixel) showing northeast trending graben (1.7–2.2 km wide) cutting the northeast flank. Also shown are irregular depressions scattered across the flank that are interpreted to be secondary craters.

6. Discussion

6.1. Composition

The visual impression of steep slopes and a bulbous morphology led some previous investigators to suggest that Tharsis Tholus had a more silicic composition than the other Tharsis volcanoes, all of which are probably basaltic shield volcanoes (Hodges and Moore, 1994; Plescia, 2003). However, the morphology of the volcano (Fig. 1) and the flank slopes (Figs. 3 and 4) are consistent with a basaltic composition. The caldera complex is deep and well-defined, formed by down dropping of blocks along concentric normal faults. This style of caldera formation is typical of terrestrial and martian basaltic shield volcanoes. Flank slopes (7° to 17°)

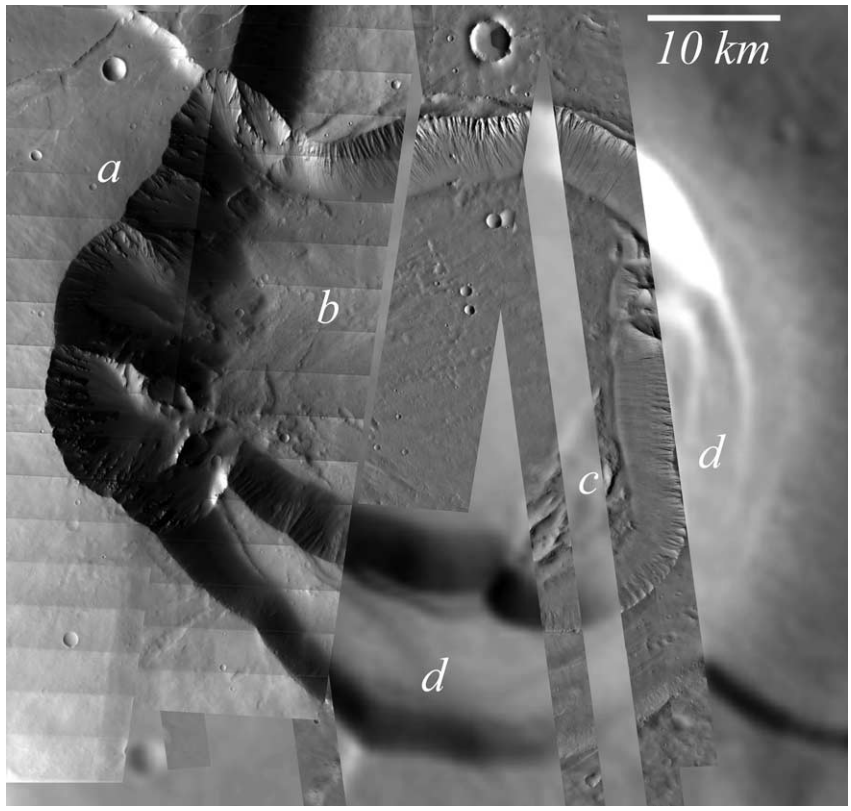

Fig. 15. Caldera interior showing the dissected western wall at "a" with bedrock ridges, debris apron at base of the slope at "b," smaller landslide at " c," and pieces of the an older caldera floor ("d") locally down-dropped on the eastern margin. Images include THEMIS V01164007 (resolution 19 m/pixel), V0863003 (resolution 19 m/pixel) and MOC image SP2-43405 (resolution 7.75 m/pixel), M04-03513 (resolution 2.95 m/pixel), and M03-00801 (resolution 7.36 m/pixel) on a low resolution MOC image base.

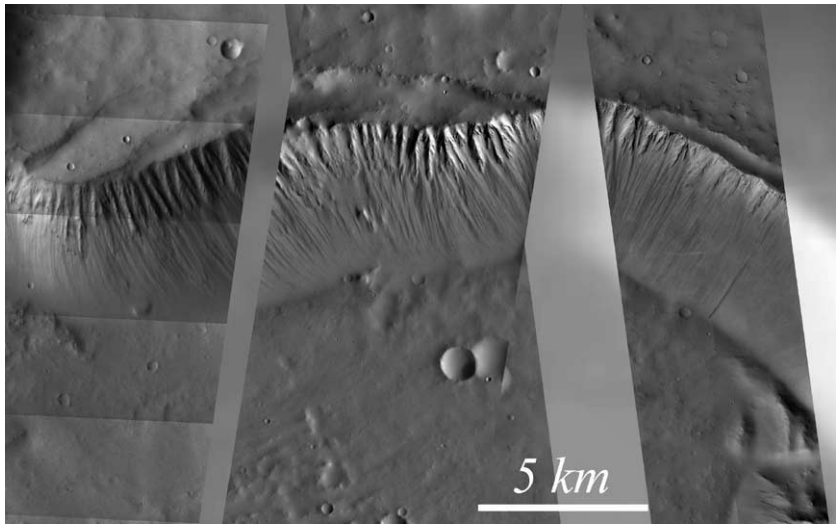

Fig. 16. North wall of the caldera showing typical wall morphology: steep upper slope—presumably exposed bedrock—and gentle lower slope—presumably a talus slope. Both the flank and the caldera floor are mantled. Note small piece of perched caldera floor at the top of the wall. Images include THEMIS V01164007 (resolution 19 m/pixel), V01863003 (resolution 19 m/pixel), MOC SP2-43404 (resolution 7.75 m/pixel), M04-03513 (resolution 2.95 m/pixel), and M03-00801 (resolution 7.36 m/pixel).

are also consistent with a basaltic composition. Cullen et al. (1987), for example, illustrate topographic profiles across the Galapagos shield volcanoes: Darwin, Fernandina, and Wolf. Each has a convex profile and maximum slopes of 24°, 26°, 23°, respectively. These are steep with respect to those observed on Hawaiian shields, yet these volcanoes are all basaltic shields. The steeper slopes of the Galapagos volcanoes have been suggested to be the result of intrusion

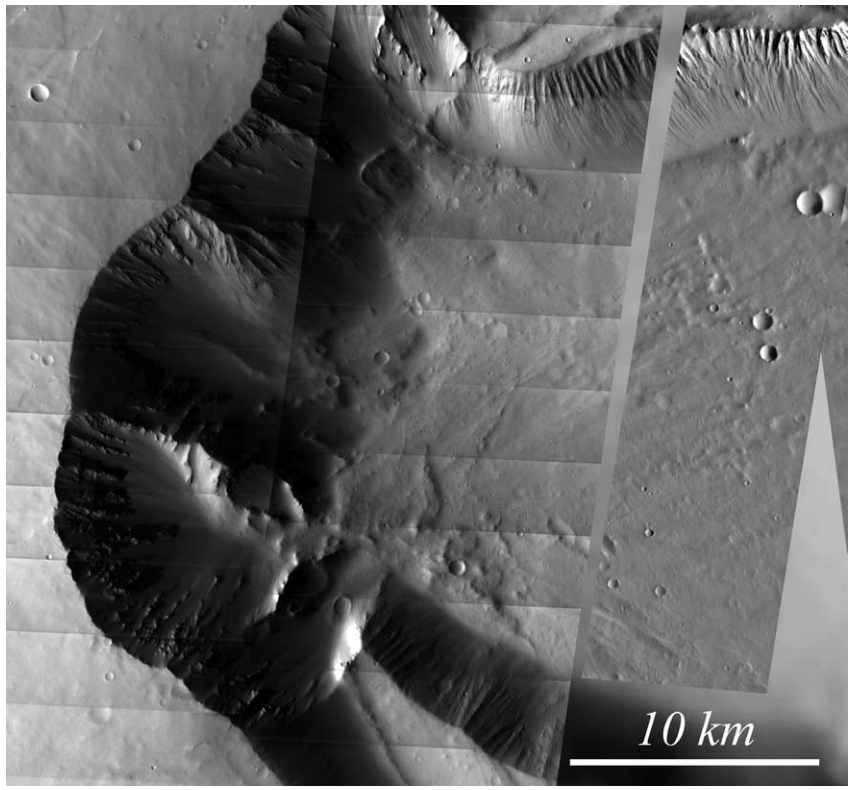

Fig. 17. Western wall of the caldera showing the scalloped amphitheater-shaped walls, linear bedrock ridges and landslide apron on the caldera floor. Images include, from left to right: THEMIS V01164007 (resolution 19 m/pixel), V0863003 (resolution 19 m/pixel) and MOC image SP2-43405 (resolution 7.75 m/pixel).

(Nordlie, 1973; Cullen et al., 1987) and intrusion could also be responsible for the relatively steep slopes on Tharsis Tholus. No explicit evidence for more silicic or explosive volcanism is observed on Tharsis Tholus as has been suggested for other martian volcanoes (e.g., Mouginis-Mark, 2002; Edgett, 1997). The material that mantles the surface appears similar to mantling material observed across the surface of Mars and is presumably the result of deposition of windblown materials rather than direct deposition of volcanic ash.

6.2. Deformation

The numerous faults indicate that Tharsis Tholus has experienced significant deformation. Tharsis Tholus does not show concentric graben as observed on the flanks of Arsia, Pavonis, and Ascraeus Mons. Obvious linear rift zones, as occur on Hawaiian or the Canary Island volcanoes, or the parasitic eruptive centers in reentrants on the Tharsis Montes shields are also absent. Extrusive volcanism appears to have been localized from the summit caldera region.

Many volcano loading and deformation models (e.g., Comer et al., 1985; McGovern and Solomon, 1993; Borgia, 1994) predict that the upper flank of a volcano should experience compression and the region beyond the volcano margin should experience radial tension. These stresses would be expected to produce circumferential thrust faults high on the flank and circumferential normal faults around the margin. Tharsis Tholus shows no evidence of circumferential compression or extension on the edifice. The absence of such loading-induced faulting indicates that the volcano did not experience the same type or magnitude of stress or it was strong enough that it did not deform under the stresses. The normal faults around the caldera are not considered be due to the volcano loading stresses but rather directly related to caldera formation and collapse (Mouginis-Mark and Rowland, 2001; Mouginis-Mark et al., 1992; Crumpler et al., 1996; Gudmundsson, 1988; Macdonald, 1965).

The large normal faults that have broken the construct into a several large intact pieces are different from those observed on any of the other martian volcanoes. Robinson and Rowland (1994) and Robinson (1993) have suggested that the such faulting is indicative of large-scale sector collapse.

Sector collapse on terrestrial volcanoes usually involves large sections of the flank being disrupted by landslides. It is typically associated with composite volcanoes and results from a weakening of the edifice due to magma intrusion, earthquakes, or hydrothermal alteration such that the flank strength is reduced allowing failure of the flank. Volcanoes of the Canary Islands display numerous horseshoe-shaped valleys that are attributed to giant landslides (Carrecedo, 1994). Similarly, such sector collapse has occurred at Casita volcano in Nicaragua (van Wyk de Vries et al., 2000) and on Piton de la Fournaise on Reunion Island (Duffield et al.,

1982) producing large amphitheater-shaped scars. In these cases, the volcano flank has been weakened and catastrophically collapses under its own weight into a disaggregated mass. This type of collapse leaves obvious scars and associated deposits, a morphology not observed on Tharsis Tholus. Thus, this type of deformation is not considered to be the cause of the large normal faults.

Deformation of Tharsis Tholus is also different from that occurring on Kilauea where the southern flank is moving seaward along a basal decollement, presumably within or along the original marine sediment/extrusive volcanic contact (e.g., Got et al., 1994; Denlinger and Okobu, 1995; Yin and Kelly, 2000). Sliding in this case occurs only in a southerly direction because the northern flank of Kilauea is buttressed against Mauna Loa. Kilauea's south flank is moving seaward at several centimeters per year along a fault that dips back beneath the volcano at an angle of a few degrees. The driving force for the displacement is suggested to be dike intrusion along the east and southwest rift zones. As a result of seaward movement of the flank, the extensional structures of the Koae and Hilina fault systems have developed. The style and cause of deformation at Kilauea do not appear to be analogs for that observed on Tharsis Tholus as there are no apparent intrusive/extrusive rift zones on Tharsis Tholus.

Large-scale brittle failure of the entire volcano may be the result of slip along a weak layer at depth or the interaction of a regional stress field with that due to the loading by the edifice. Several studies have examined the influence of regional subsurface faults and ductile layers on the deformation of a volcano.

Lagmay et al. (2000) and van Wyk de Vries and Merle (1998) investigated the effects of strike-slip faulting on the deformation of volcanoes. They found in mechanical and numerical experiments that an extensional environment develops at the summit. Depending upon the amount of movement along the strike-slip fault at depth and the mechanical properties of the various units, the deformation can range from a simple sigmoidal normal fault across the volcano to a well-defined graben oriented at an angle to the strike of the underlying fault; a radial geometry does not develop. This is not the style of deformation observed at Tharsis Tholus and obvious strike-slip faults are absent in this part of Tharsis; hence this model is probably not applicable.

van Wyk de Vries and Merle (1996) conducted experiments of a volcanic cone overlying an extensional fault to investigate the effects of the extension on the volcano and the influence of the volcano of the regional fault patterns. Their model assumed a single extensional fault beneath the volcano as well as a ductile layer at depth. As a result of the load, regional fault patterns curve into the volcano producing a set of normal faults on the edifice that are at an angle to the regional trend. Depending upon the ratio of the thickness of the ductile to rigid layer, that angle changes; as the ratio of brittle layer thickness to ductile layer thickness decreases the angle of the faults increase with respect to the regional direction. The large normal faults at Tharsis Tholus are arcuate but have average trends producing an angle of 5° and 65° with respect to the trend of the regional graben. This would suggest a similar brittle and ductile layer thickness. These models suggest that a major subsurface fault beneath Tharsis Tholus might be the cause of the large normal faults. However, the presence of the narrow graben on the edifice parallel to the strike of the regional faults may indicate that the stresses that produced the graben have propagated through the edifice with no deflection making this model inapplicable to Tharsis Tholus.

Volcanoes deforming under their own mass develop characteristic radial summit faults. Several studies (van Wyk de Vries and Borgia, 1996; Merle and Borgia, 1996; van Wyk de Vries and Matela, 1998; Borgia et al., 2000) have examined the styles of deformation through numerical modeling of the volcano and underlying brittle and ductile layers. Several volcanoes in the Central American volcanic arc, having a variety of basement lithologies and styles and magnitudes of deformation, were compared. These studies suggest that volcanoes built on weak substrate and those that are rapidly built are the most susceptible to deformation. They show that a volcano loading a deep ductile layer causes the ductile layer to spread. As the ductile layer thickness increases or the rigid layer decreases, the likelihood of spreading increases.

A terrestrial analog for Tharsis Tholus, in the context of such models is the Maderas Volcano in Nicaragua (Fig. 18). Maderas is constructed of interlayered pyroclastics and lava, stands $\sim$ 1.4 km high, is 10 km across and has average flank slopes up to 25° with more gentle slopes in the summit region (van Wyk de Vries and Borgia, 1996). It is built on Quaternary sediments of Lake Nicaragua overlying a deeper basement of oceanic rocks. Several large normal faults having offsets of the order 150 m cut the volcano into a series of half graben with a prominent irregular graben cutting across the summit. The deformation is the result of loading by the volcano on a weak substratum.

The deformation of Tharsis Tholus resembles that of Maderas in that the edifice is broken into several large blocks. This similarity in morphology suggests the possibility of an analogous failure mechanism. If the model is applicable to Tharsis Tholus, a subsurface low-strength layer must exist. The weak layer might be the Noachian-age heavily cratered basement, although the depth to this unit and its properties are unknown. Perhaps the brecciated cratered material is ice- or water-rich allowing it to behave in a ductile manner.

An interesting small-scale analog for the deformation of Tharsis Tholus may be found in the Toreva blocks of the Colorado Plateau (Reiche, 1937; Rogers, 1991). Here, blocks of Mesa Verde sandstone (typically 300–500 m across) are sliding, intact although rotated, over the nearly flat lying Mancos Shale.

van Wyk de Vries and Matela (1998) also illustrate that under different viscosity conditions thrust faults can be gen-

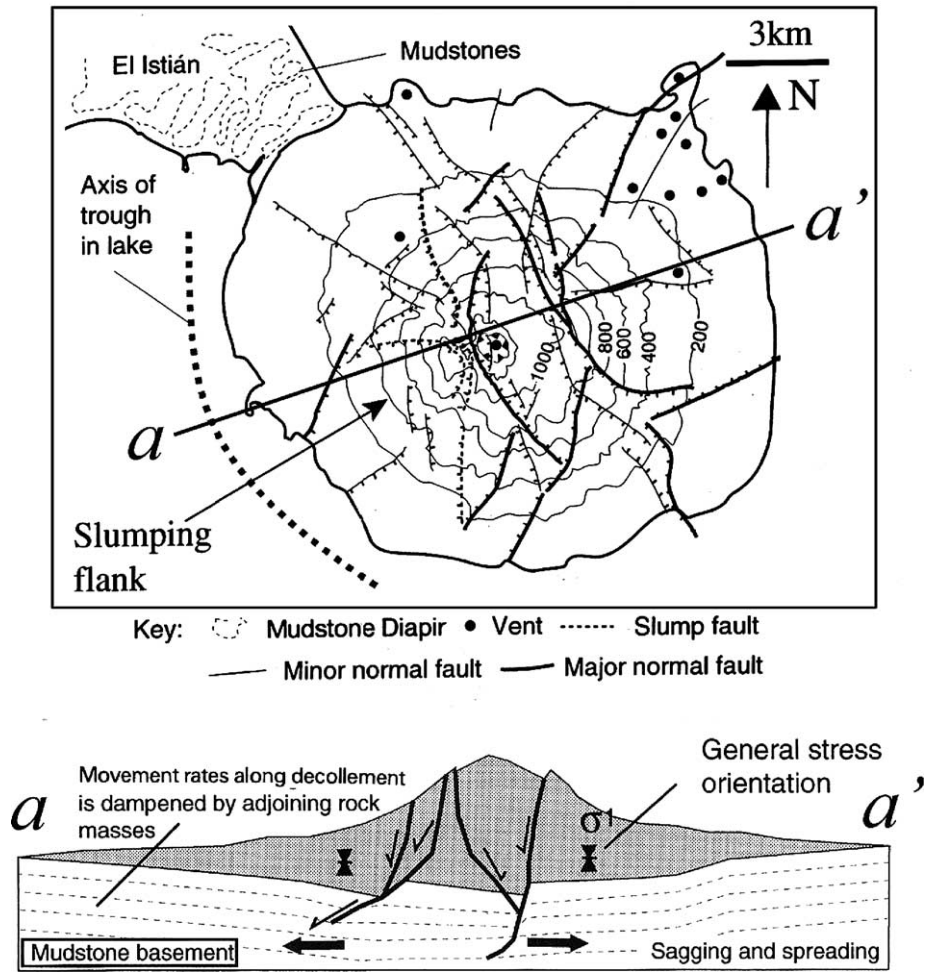

Fig. 18. Structural map of the Maderas Volcano (from van Wyk de Vries and Borgia, 1996). Upper panel shows the map view of the volcano with numerous graben cutting the volcano surface. Low panel shows a cross section illustrating the proposed geometry of the faults cutting through the edifice and into the underlying mudstone basement.

erated at the base of a volcanic edifice. In one model, they illustrate the base of a volcano being pushed out and over a ductile layer. The edge of the volcano above the thrust breaks-up along normal faults into a few closely spaced blocks. This model may provide an explanation for the blocks on the northwest flank of Tharsis Tholus. Such an event might have occurred when the ductile material was well coupled to the volcano and the flow of the ductile material dragged the volcano with it.

Narrow graben have a consistent northeast trend across the volcano suggesting they are due to a regional rather than local stress system. A stress system having a northwest extension direction in this part of Tharsis is consistent with a Tharsis-centered stress system (Banerdt et al., 1992). The strike of these faults (55° N–65° E) points back toward Pavonis Mons. Pavonis Mons is coincident with one of the loci of regional faulting that have been defined for the Tharsis region (Plescia and Saunders, 1982; Anderson et al., 2001). Based on the average Early Hesperian age of the flanks of Tharsis Tholus (see below), these faults would correspond with the "Pavonis I" phase of faulting defined by Plescia and Saunders (1982). However, younger faulting associated with the "Pavonis II" phase would probably not be applicable since the surrounding volcanic plains are not cut by the faults.

A possible chronology for fault formation would be: formation of some northeast trending graben, formation of the large normal faults breaking the entire edifice, renewed/continued volcanism which buried the distal down slope ends of the eastern faults, and then renewed northeast trending graben formation.

6.3. Flank burial

The flanks of Tharsis Tholus are clearly embayed by the younger volcanic plains. The amount of burial is, however, uncertain. On the basis of caldera diameter/volcano diameter data (Pike, 1978; Pike and Clow, 1981), Whitford-Stark (1982) suggested the flanks of Tharsis Tholus were buried by $\sim$ 850 m of younger material. If true, the total edifice would be about 20% wider. Robinson (1993) suggested 3.5 km of burial based on analogies to terrestrial volcano dimensional

ratios which suggest a considerably greater diameter for the original construct.

The only data point that provides a constraint on the thickness of the surrounding plains in the immediate vicinity is from a partially buried crater east of the volcano (Fig. 1). That crater has an apparent diameter of ~ 47 km, based on an exposed arcuate piece of pre-plains bedrock. However, the eastern flank of Tharsis Tholus also has a concave boundary that might represent the actual crater rim, in which case the 47 km diameter feature is an interior ring and the actual crater diameter is ~ 70 km. Using crater rim height relations for martian craters based on MOLA data (Garvin et al., 2000) the original rim height would have been 430–520 m (for a crater 47–70 km in diameter). Given that some tens of meters of rim remains exposed and that the rim height could have been reduced by erosion, a maximum thickness of the plains would be on the order of 500 m. Regional studies (Plescia and Saunders, 1980) also suggest that around the margins of the Tharsis uplift the extrusive volcanics are a relatively thin (hundreds of meters as opposed to kilometers).

Assuming a 15° flank slope, a layer of lava 500 m thick would reduce the volcano radius by only ~ 2 km. Thus, the edifice would not have been much wider before being embayed. In the cases of the other small volcanoes in Tharsis, it has been suggested (Plescia, 1994, 2000) that the reason the morphometric ratios are different from those of terrestrial volcanoes is not that they are buried to a significant degree, but simply that the calderas are relatively large in the older smaller martian shield volcanoes, perhaps due to a relatively large magma chambers. A similar situation may hold for Tharsis Tholus.

7. Chronology

Crater counts were made to determine the stratigraphic position of Tharsis Tholus. Counts of the flank were made using Viking and MOC images; for the caldera using MOC images; and for the surrounding plains using Viking images. Table 2 lists the summaries of these counts. Counts using the three sets of Viking images overlap at the four diameters listed. The variation in counts between the different image sets is probably the result of differences in crater recognition and the statistics of the low number of craters and small areas. The largest variations occur at 1 km which represents only 4–5 pixels in the Viking 858A and 857A images.

Figure 19 illustrates the cumulative size-frequency plot for the Viking 669A images. It can be seen that the curve has an inflection around 3 km indicating that two populations of craters occur on the surface, consistent with resurfacing of the flank. Cumulative frequency values derived

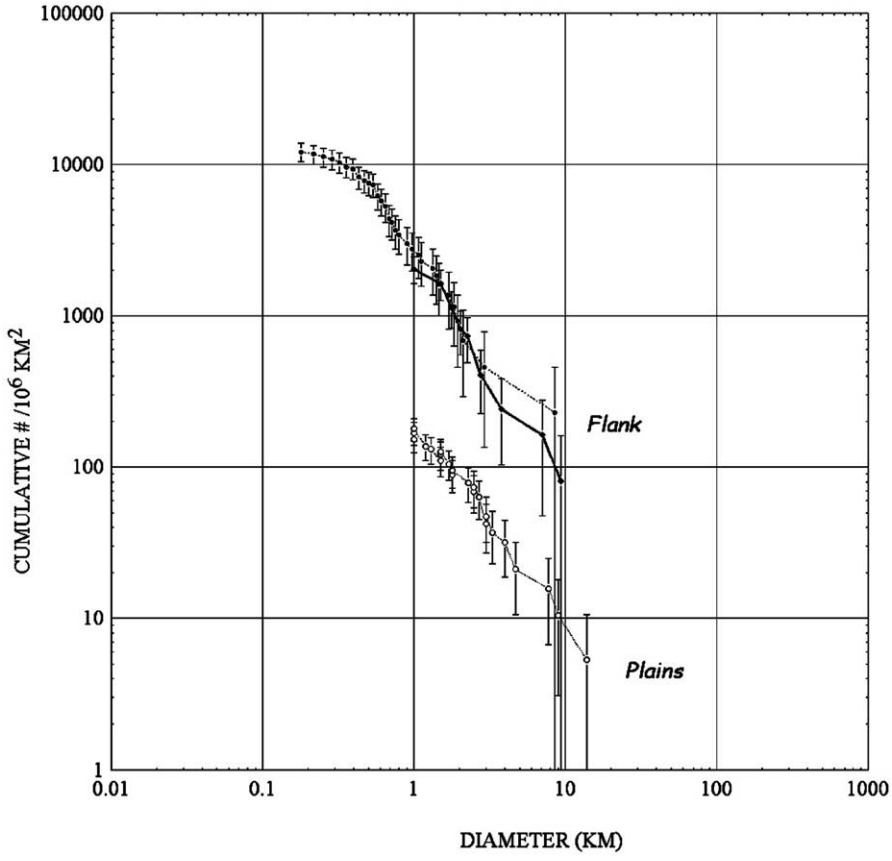

Fig. 19. Cumulative size-frequency distribution of craters on the flank and adjacent plains. Upper two curves (filled symbols) show counts for the flank derived from Viking frames 857A51 and 669A11-16. Dashed line with open circles illustrates counts for surrounding plains from Viking images 857A49-52.

Table 2
Morphometric data for Tharsis Tholus

Parameter	Value
Location	13.5° N–91° W
Edifice dimensions	158 × 131 km
Caldera dimensions	48 × 47 km
Maximum summit elevation	+9 km
Caldera floor elevation	+2.2–3.2 km
Caldera depth relative to Rim	2.5–7 km
Relief	7–8 km
Volume	22.1×10^3 km^3
Flank slope	3–15°

from Viking images indicate the flank of Tharsis Tholus has an Early Hesperian age, using $N(2)$ and the chronology of Tanaka et al. (1992). This places Tharsis Tholus in a time period older than the Uranius Group of volcanoes to the north, which are Late Hesperian in age, and contemporaneous with Biblis Patera and Ulysses Patera on the west side of Tharsis, which are approximately Early Hesperian in age (Plescia 1994, 2000; Neukum and Hiller, 1981; Plescia and Saunders, 1979).

The surrounding plains are assigned to Member 5 of the Tharsis Montes Formation (Scott and Tanaka, 1986). Scott et al. (1981) define he surrounding plains as part of the Tharsis Montes flows with crater frequencies of $N(1) = 430$–570. Counts compiled during this study for the area immediately surrounding the volcano indicate $N(1)$ of 179 ± 31 and $N(2)$ of 85 ± 21 (Table 3), considerably younger than the data from Scott et al. (1981). These new counts place the surrounding plains in the Middle Amazonian, although still within the range of ages indicated for Member 5 of the Tharsis Montes Formation by Scott and Tanaka (1986).

Counts derived from the MOC image are considerably at odds with those from Viking images indicating cumulative frequencies at $\geqslant 1$ km up to an order of magnitude greater than those calculated using the Viking images. The MOC images have a very high resolution and cover only a very small area (see Table 2). The largest crater observed is 2.89 km; a total of 4 craters > 1 km are observed. It is suggested that the very high normalized (to 10^6 km^2) cumulative values result from the very small counting area, the few number of relevant craters, and a possible upturn of the slope of size-frequency distribution at < 1 km. The possibility that the small-diameter craters observed in MOC images may have a significant contribution from secondary craters has recently been suggested by McEwen et al. (2003). If secondary craters do significantly affect the population of craters in the tens to hundreds of meter diameter, then the size-frequency distribution would have a significant upturn at diameters below 1 km. The extent and presence of the upturn might also be spatially variable and related to young large craters nearby.

Thus, counts at diameters of tens to a few hundred meters cannot be linearly extrapolated to multi-kilometer diameters. At this point in time, counts from MOC images are not considered to be directly comparable with those from Viking images and cannot be used for stratigraphic delineation.

8. Conclusions

Tharsis Tholus is unique among the other martian shield volcanoes. It has faults which are associated with regional extension (northeast trending graben) and with failure of the entire edifice due to loading (the large normal faults). The morphology of the edifice is consistent with that of a basaltic shield volcano, but definitive volcanic morphology is hidden by an aeolian surficial mantle. Crater counts indicate an age of Early Hesperian, placing it in the middle of the period of small edifice development in Tharsis.

Acknowledgment

Reviews of the submitted manuscript by David Crown and an anonymous reviewer are appreciated as they pointed out a number of instances where the discussion could be better focused or expanded. Reviews by Wendell Duffield and Jeffrey Johnson of the draft manuscript were also quite helpful. This research was supported by the NASA Planetary Geology and Geophysics Program.

Table 3
Crater counts for Tharsis Tholus

Image set	$N(1)$	$N(2)$	$N(5)$	$N(10)$	N	Res	Area
Viking							
Flank							
669A11-16	2696 ± 788	839 ± 439	(192 ± 210)	(63 ± 120)	53	23	4,348
858A23	2471 ± 52	697 ± 240	202 ± 129	(34 ± 53)	33	186	12,101
857A51	(3837 ± 560)	832 ± 260	204 ± 129	(33 ± 52)	25	252	12,274
MOC 43405							
Caldera	6787 ± 6208	(3741 ± 4608)	(981 ± 2360)		178	8	176
Flank	24077 ± 11509	13493 ± 8616	(15002 ± 9085)		205	8	182
Surrounding plains							
857A49-52	179 ± 31	85 ± 21	20 ± 10	9 ± 7	34	250	189,928

$N(D)$ indicates the cumulative number of crater $\geqslant D$ km per 10^6 km^2. N is the number of craters counted; Res is the image resolution in meters/pixel; area is the counting area in km^2. Numbers in parentheses represent extrapolations to smaller or larger diameters beyond the observed data using a visually fit line. Uncertainties are calculated assuming they are related to the square root of the number of craters counted.

Appendix A
Images of Tharsis Tholus

PICNO	Clat	Clong	Inc.	Scale
090A61	12.93	92.3	7.88	50
090A62	12.49	91.43	8.52	49
090A63	13.45	91.31	7.67	49
090A64	12.89	90.49	8.5	48
090A65	13.8	90.38	7.74	48
090A66	13.27	89.54	8.61	48
225A10	10.75	95.06	43.82	138
225A12	10.92	92.5	46.26	136
225A13	13.21	92.08	47.5	136
225A14	11.07	90.1	48.55	134
225A15	13.3	89.74	49.68	134
225A16	11.21	87.81	50.75	132
357B08	14.5	88.81	69.96	48
444A06	11.3	94.82	53.03	441
444A07	17.25	95.62	55.15	444
444A09	11.56	93.32	54.52	440
444A24	17.51	91.89	58.86	437
444A26	11.64	89.76	58.23	433
444A27	17.21	90.31	60.11	436
444A29	11.29	88.33	59.43	325
682A01	12.78	91.52	75.65	325
682A22	15.56	87.8	70.6	335
699A08	13.79	92.39	72.52	36
699A09	14.08	91.88	72.89	36
699A10	13.34	91.85	73.21	36
699A11	13.61	91.34	73.58	36
699A12	12.85	91.29	73.94	36
699A13	13.15	90.8	74.28	36
699A14	12.39	90.73	74.65	36
699A15	12.67	90.22	75.02	36
699A16	11.91	90.14	75.4	36
699A42	14.00	92.22	73.41	23
699A43	14.22	91.84	73.68	23
699A44	13.8	91.92	73.79	23
699A45	14.00	91.53	74.07	23
699A46	13.58	91.62	74.18	22
701A03	13.91	89.94	59.75	776
857A49	17.24	89.25	71.33	249
857A52	12.94	93.41	75.52	252
858A21	14.03	93.86	79.57	189
858A42	11.62	92.67	77.85	181
858A44	11.37	89.62	74.85	178
858A46	11.07	86.28	71.57	176
SP1-23106	13.91	92.31	46.42	3.15
SP2-43405	13.89	91.15	79.05	7.75
M03-00801	13.78	90.99	39.04	7.36
M03-04592	14.32	92.08	40.88	2.94
M03-05935	12.55	90.65	41.21	5.86
M04-03513	13.94	91.17	44.16	2.95
M07-01844	14.47	89.45	45.76	1.47
M07-04361	14.23	91.94	46.72	2.95
M07-05895	13.74	90.95	47.02	5.88
M08-04702	14.15	92.54	48.37	2.94
M14-00732	12.62	91.52	28.89	4.44
E03-01974	1359	91.05	36.95	8.85
E08-01290	13.62	91.36	48.71	6.20
E09-01814	13.68	91.79	48.08	6.21
E10-03774	12.65	91.62	44.59	6.18
E11-01780	14.38	89.81	43.91	3.11
E12-00031	14.00	92.35	40.25	4.66
E12-01907	13.84	90.11	37.28	6.20
E13-00672	14.08	92.49	33.64	6.20
E14-00541	13.60	91.52	28.21	6.21
I00871005	20.556	91.571	136.06	102
I01164006	6.718	92.535	49.314	101
I01233003	21.169	91.857		
I01863002	21.171	90.004	54.455	102
I01888005	21.991	91.140	54.682	102
I02200005	14.836	90.145	55.43	102
I02319005	12.979	91.209	118.338	102
I02587006	13.485	90.751		
V01164007	13.485	91.6	51.721	19
V01863003	13.548	91.358	53.326	19
V02974007	13.689	91.474	60.991	37

Clat: Center latitude of original image. Clong: Center longitude of original image. Inc.: Incidence angle. Images listed here are those for which visibility was adequate for surface observations and does include several very low resolution (700–800 m/pixel) images.

References

Anderson, R.C., Dohm, J.M., Golombek, M.P., Haldemann, A.F.C., Franklin, B.F., Tanaka, K.L., Lias, J., Peer, B., 2001. Primary centers and secondary concentrations of tectonic activity through time in the western hemisphere of Mars. J. Geophys. Res. 106, 20563–20585.

Banerdt, W.B., Golombek, M.P., Tanaka, K.L, 1992. Stress and tectonics on Mars. In: Kieffer, H.H., Jakosky, B.M., Snyder, C.W., Matthews, M.S. (Eds.), Mars. Univ. of Arizona Press, pp. 249–297.

Borgia, A., 1994. Dynamic basis of volcanic spreading. J. Geophys. Res. 99, 17791–17804.

Borgia, A., Delaney, P., Denlinger, R.P., 2000. Spreading volcanoes. Annu. Rev. Earth Planet. Sci. 28, 539–570.

Cattermole, P., 1990. Volcanic flow development at Alba Patera, Mars. Icarus 83, 453–493.

Carr, M.H., 1973. Volcanism on Mars. J. Geophys. Res. 78, 4049–4062.

Carr, M.H., 1974. Tectonism and volcanism of the Tharsis region of Mars. J. Geophys. Res. 79, 3943–3949.

Carr, M.H., 1975. Geologic map of the Tharsis Quadrangle of Mars. US Geol. Survey Miscellaneous Investigations Series I-893. Scale 1:5,000,000.

Carrecedo, J.C., 1994. The Canary Islands: an example of structural control on the growth of large oceanic-island volcanoes. J. Volcanol. Geoth. Res. 60, 225–241.

Christensen, P.R., Jakosky, B.M., Kiefer, H.H., Malin, M.C., McSween, H.Y., Nealson, K., Mehall, G., Silverman, S., Ferry, S., 1999. The Thermal Emission Imaging System (THEMIS) instrument for the 2001 orbiter. In: Proc. Lunar Planet. Sci. Conf. 30th. Abstract 1470.

Comer, R.P., Solomon, S.C., Head, J.W., 1985. Mars: thickness of the lithosphere from the tectonic response to volcanic loads. Rev. Geophys. 23, 61–92.

Crumpler, L.S., Aubele, J.C., 1978. Structural evolution of Arsia Mons, Pavonis Mons, and Ascraeus Mons: Tharsis region of Mars. Icarus 34, 496–511.

Crumpler, L.S., Head, J.W., Aubele, J.C., 1996. Calderas on Mars: characteristics, structure and associated flank deformation. In: McGuire, W.J., Jones, A.P., Neuberg, J. (Eds.), Volcano Instability on the Earth and Other Planets, pp. 307–348. Geological Society Special Publication No. 110.

Cullen, A.B., McBirney, A.R., Rogers, R.D., 1987. Structural controls on the morphology of Galapagos shields. J. Volcanol. Geoth. Res. 34, 143–151.

Denlinger, R.P., Okobu, P., 1995. Structure of the mobile south flank of Kilauea volcano, Hawaii. J. Geophys. Res. 100, 24499–24507.

Duffield, W.A., Stieltjes, L., Varet, J., 1982. Huge landslide blocks in the growth of Piton de la Fournaise, La Reunion, and Kilauea volcano, Hawaii. J. Volcanol. Geoth. Res. 12, 147–160.

Edgett, K.S., 1997. Aeolian dunes as evidence for explosive volcanism in the Tharsis region of Mars. Icarus 130, 96–114.

Garvin, J.B., Frawley, J.J., Sakimoto, S.E.H., Schnetzler, C., 2000. Global geometric properties of martian impact craters: an assessment from Mars Orbiter Laser Altimeter (MOLA) digital elevation models. In: Proc. Lunar Planet. Sci. Conf. 31st. Abstract 1619.

Got, J.L., Frechet, J., Klein, F.W., 1994. Deep fault plane geometry inferred from multiple relative relocation beneath the south flank of Kilauea. J. Geophys. Res. 99, 15375–15386.

Greeley, R., Spudis, P., 1981. Volcanism on Mars. Rev. Geophys. 19, 13–41.

Gudmundsson, A., 1988. Formation of collapse caldera. Geology 16, 808–810.

Gulick, V., 2001. Origin of the valley networks on Mars a hydrological perspective. Geomorphology 37, 241–268.

Head, J.W., Seibert, N., Pratt, S., Smith, D., Zuber, M., Solomon, S., McGovern, P., Garvin, J., 1998a. Characterization of major volcanic edifices on Mars using Mars Orbiter Laser Altimeter (MOLA) data. In: Proc. Lunar Planet. Sci. Conf. 29th. Abstract 1322.

Head, J.W., Seibert, N., Pratt, S., Smith, D., Zuber, M., Garvin, J.B., McGovern, P.J., the MOLA Science Team, 1998b. Volcanic calderas on Mars: initial views using Mars Orbiter Laser Altimeter Data. In: Proc. Lunar Planet. Sci. Conf. 29th. Abstract 1488.

Hiesinger, H., Head, J.W., 2002. Syrtis Major, Mars: results from Mars Global Surveyor Data. In: Proc. Lunar Planet. Sci. Conf. 33rd. Abstract 1063.

Hodges, C.A., Moore, H.J., 1994. Atlas of volcanic landforms on Mars. US Geol. Survey Prof. Paper 1534, 194.

Lagmay, A.M.F., van Wyk de Vries, B., Kerle, N., Pyle, D.M., 2000. Volcano instability induced by strike-slip faulting. B. Volcanol. 62, 331–346.

Macdonald, G.A., 1965. Hawaiian calderas. Pac. Sci. 19, 320–334.

Malin, M.C., Danielson, G.E., Ingersoll, A.P., Masursky, H., Veverka, J., Ravine, M.A., Soulanill, T.A., 1992. Mars Observer Camera. J. Geophys. Res. 97, 7699–7718.

Malin, M.C., Edgett, K.S., 2001. Mars Global Surveyor Mars Orbiter Camera: interplanetary cruise through primary mission. J. Geophys. Res. 106, 23429–23570.

Merle, O., Borgia, A., 1996. Scaled experiments of volcanic spreading. J. Geophys. Res. 101, 13805–13817.

McEwen, A., Turtle, E., Burr, D., Milazzo, M., Lanagan, P., Christensen, P., Boyce, J., 2003. Discovery of a large rayed crater on Mars: implications for recent volcanic and fluvial activity and the origin of martian meteorites. In: Proc. Lunar Planet. Sci. Conf. 34th. Abstract 2040.

McGovern, P., Solomon, S.C., 1993. State of stress, faulting, and eruption characteristic of large volcanoes on Mars. J. Geophys. Res. 98, 23553–23579.

Moore, J.G., Bryan, W.B., Beeson, M.H., Normark, W.P., 1995. Giant blocks in the south Kona landslide, Hawaii. Geology 23, 125–128.

Moore, J.G., Clague, D.A., Holcomb, R.T., Lipman, P.W., Normark, W.R., Torresan, M.E., 1989. Prodigious submarine landslides on the Hawaiian ridge. J. Geophys. Res. 94, 17465–17484.

Morris, E.C., Tanaka K.L., 1994. Geologic maps of the Olympus Mons region, US Geol. Survey Miscellaneous Investigation Series Maps I-2327.

Mouginis-Mark, P.J., 2002. Prodigious ash deposits near the summit of Arsia Mons volcano, Mars. Geophys. Res. Lett. 29. 10.1029/2002GL015296.

Mouginis-Mark, P.J., Kallianpur, K.J., 2002. Heights of martian volcanoes and the geometry of their calderas from MOLA data. In: Proc. Lunar Planet. Sci. Conf. 33rd. Abstract 1409.

Mouginis-Mark, P.J., Rowland, S.K., 2001. The geomorphology of planetary calderas. Geomorphology 37, 201–223.

Mouginis-Mark, P.J., Wilson, L., Zuber, M.T., 1992. The physical volcanology of Mars. Chapter 13. In: The Mars Book. Univ. of Arizona Press, Tucson, pp. 424–452.

Naka, J., 34 others, 2000. Tectono-magmatic processes investigated at deep-water flanks of Hawaiian volcanoes. EOS 221, 226–227.

Neukum, G., Hiller, K., 1981. Martian ages. J. Geophys. Res. 86, 3097–3121.

Nordlie, B.E., 1973. Morphology and structure of the western Galapagos volcanoes and a model for their origin. Geol. Soc. Am. Bull. 84, 2931–2956.

Okubo, C.H., Martel, S.J., 1998. Pit crater formation on Kilauea volcano, Hawaii. J. Volcanol. Geoth. Res. 86, 1–18.

Pike, R., 1978. Volcanoes on the inner planets: some preliminary comparisons of gross topography. In: Proc. Lunar Planet. Sci. Conf. 9th, pp. 3239–3273.

Pike, R., Clow, G., 1981. Revised classification of terrestrial volcanoes and catalog of topographic dimensions with new results on edifice volume. US Geol. Survey Open File Report 81-1038, 40 pp.

Plescia, J., 1994. Geology of the small Tharsis volcanoes: Jovis Tholus, Ulysses Patera, Biblis Patera, Mars. Icarus 111, 246–269.

Plescia, J., 2000. Geology of the Uranius group volcanic constructs: Uranius Patera, Ceraunius Tholus, and Uranius Tholus. Icarus 143, 376–396.

Plescia, J., 2003. Morphometric properties of martian volcanoes. J. Geophys. Res. Submitted.

Plescia, J.B., Saunders, R.S., 1979. The chronology of the martian volcanoes. In: Proc. Lunar Planet. Sci. Conf. 10th, pp. 2841–2859.

Plescia, J., Saunders, R.S., 1980. Estimation of the thickness of the Tharsis lava flows and implications for the nature of the topography of the Tharsis plateau. In: Proc. Lunar Planet. Sci. Conf. 11th, pp. 2423–2436.

Plescia, J., Saunders, R.S., 1982. Tectonic history of the Tharsis region, Mars. J. Geophys. Res. 87, 9775–9791.

Reiche, P., 1937. The Toreva block—a distinctive landslide type. J. Geology 45, 538–548.

Robinson, M., Rowland, S., 1994. Evidence for large scale sector collapse at Tharsis Tholus. Conference on Volcano Instability on Earth and Other Planets. Geological Society of London. 44.

Robinson, M., 1993. Some aspects of lunar and martian volcanism as examined with spectral, topographic, and morphologic data derived from spacecraft images. University of Hawaii. Dissertation, pp. 257.

Rogers, J., 1991. Toreva block mega-landslides in the Colorado River channel, Grand Canyon Arizona. Geol. Soc. Am. Abstracts with Prog. 23, 126.

Sakimoto, S.E.H., Gregg, T.K.P., Hughes, S.S., Chadwick, J., 2003. Martian plains volcanism in Syria Planum and Tempe Mareotis as analogs to the eastern Snake River Plains Idaho: similarities and possible petrologic contributions to topography. In: Proc. Lunar Planet. Sci. Conf. 34th. Abstract 1740.

Scott, D.H., Zimbelman J.R., 1995. Geologic map of Arsia Mons volcano, Mars. US Geol. Survey Miscellaneous Investigation Series I-2480.

Scott, D.H., Dohm, J.M., Zimbelman, J.R., 1998. Geologic map of Pavonis Mons volcano, Mars. US Geol. Survey Miscellaneous Investigations Series I-2561.

Scott, D.H., Schaber, G.G., Tanaka K.L., 1981. Map showing lava flows in the southeast part of the Tharsis Quadrangle of Mars. US Geol. Survey Miscellaneous Investigations Series I-1269. Scale 1:2,000,000.

Scott, D.H., Tanaka K.L., 1986. Geologic map of the western equatorial region of Mars. US Geol. Survey Miscellaneous Investigations Map I-1802A. Scale 1:15,000,000.

Shepard, M.K., Campbell, B.A., Bulmer, M.H., Farr, T.G., Gaddis, L.R., Plaut, J.J., 2001. The roughness of natural terrain: a planetary and remote sensing perspective. J. Geophys. Res. 106, 32777–32795.

Smith, D.E., 23 others, 2001. Mars orbiter laser altimeter: experiment summary after the first year of global mapping on Mars. J. Geophys. Res. 106, 23689–23722.

Tanaka, K.L., Scott, D.H., Greeley, R., 1992. Global stratigraphy. In: Kieffer, H.H., Jakosky, B.M., Snyder, C.W., Matthews, M.S. (Eds.), Mars. Univ. of Arizona Press, pp. 345–382.

US Geol. Survey, 1989. Topographic maps of the western, eastern equatorial and polar regions of Mars. US Geol. Survey Miscellaneous Investigations Series I-2030.

US Geol. Survey, 1991. Topographic map of the Tharsis northeast quadrangle (MC-9NE) of Mars. US Geol. Survey Miscellaneous Investigation Series Map I-2111.

van Wyk de Vries, B., Borgia, A., 1996. The role of basement in volcano deformation. in Volcano instability on the Earth and Other Planets. Geol. Soc. Spec. Publ. 110, 95–110.

van Wyk de Vries, B., Matela, R., 1998. Styles of volcano-induced deformation: numerical models of substratum flexure, spreading, and extrusion. J. Volcanol. Geoth. Res. 81, 1–18.

van Wyk de Vries, B., Kerle, N., Petley, D., 2000. Sector collapse forming at Casita volcano, Nicaragua. Geology 28, 167–170.

van Wyk de Vries, B., Merle, O., 1996. The effect of volcanic constructs on rift fault patterns. Geology 24, 643–646.

van Wyk de Vries, B., Merle, O., 1998. Extension induced by volcanic loading in regional strike slip zones. Geology 26, 983–986.

Whitford-Stark, J., 1982. Tharsis volcanoes: separation distances, relative ages, sizes, morphologies, and depths of burial. J. Geophys. Res. 87, 9829–9838.

Yin, A., Kelly, T.A., 2000. An elastic wedge model for the development of coeval normal and thrust faulting in the Mauna Loa-Kilauea rift system in Hawaii. J. Geophys. Res. 105, 25909–25925.

Zuber, M., Smith, D., Solomon, S., Muhleman, D., Head, J., Garvin, J., Abshire, Bufton, J., 1992. The Mars Observer Laser Altimeter investigation. J. Geophys. Res. 97, 7781–7798.